Molecular Photoacoustic Imaging of Follicular Thyroid Carcinoma

Jelena Levi[1,2], Sri-Rajashekar Kothapalli[2], Sarah Bohndiek[2], Joon-Kee Yoon[3], Anca Dragulescu-Andrasi[2], Carsten Nielsen[2], Aleksandra Tisma[4], Sunil Bodapati[2], Gayatri Gowrishankar[2], Xinrui Yan[2], Carmel Chan[2], Daniela Starcevic[2], and Sanjiv Sam Gambhir[1,2]

Abstract

Purpose: To evaluate the potential of targeted photoacoustic imaging as a noninvasive method for detection of follicular thyroid carcinoma.

Experimental Design: We determined the presence and activity of two members of matrix metalloproteinase family (MMP), MMP-2 and MMP-9, suggested as biomarkers for malignant thyroid lesions, in FTC133 thyroid tumors subcutaneously implanted in nude mice. The imaging agent used to visualize tumors was MMP-activatable photoacoustic probe, Alexa750-CXeeeeXPLGLAGrrrrrXK-BHQ3. Cleavage of the MMP-activatable agent was imaged after intratumoral and intravenous injections in living mice optically, observing the increase in Alexa750 fluorescence, and photoacoustically, using a dual-wavelength imaging method.

Results: Active forms of both MMP-2 and MMP-9 enzymes were found in FTC133 tumor homogenates, with MMP-9 detected in greater amounts. The molecular imaging agent was determined to be activated by both enzymes *in vitro*, with MMP-9 being more efficient in this regard. Both optical and photoacoustic imaging showed significantly higher signal in tumors of mice injected with the active agent than in tumors injected with the control, nonactivatable, agent.

Conclusions: With the combination of high spatial resolution and signal specificity, targeted photoacoustic imaging holds great promise as a noninvasive method for early diagnosis of follicular thyroid carcinomas. *Clin Cancer Res; 19(6); 1494–502. ©2013 AACR.*

Introduction

In the United States, thyroid cancer has a lower incidence and mortality rate than other cancers (1). While thyroid cancers are rare, benign thyroid nodules are very common and discriminating between them is essential for proper patient management. Three of 4 types of thyroid cancer can be accurately diagnosed using current clinical diagnostic methods that use ultrasound and fine-needle aspiration cytology (FNAC) to determine cytologic features indicating malignant cell transformations. However, because of its cytologic similarity to benign adenoma, follicular thyroid carcinoma still presents a diagnostic challenge. Most often the only clear distinction between the follicular thyroid carcinoma and adenoma is the vascular and capsular invasion that can be detected only after partial or complete removal of the thyroid. As benign nodules are overwhelmingly prevalent, 70% to 80% of all surgical removals will prove to be unnecessary (2). Inclusion of a noninvasive imaging method in the clinical decision process would potentially bring considerable benefit to patient management and reduce the healthcare costs associated with unnecessary thyroid removals. Molecular imaging has a significant role in cancer research as a tool that enables better understanding of this disease and thus could offer insight into and improvement of various areas of cancer care (3, 4). One of the molecular imaging modalities, photoacoustic imaging, has experienced an extremely rapid growth over the recent years due to the many potential advantages it offers (5). Photoacoustic imaging, with its good tissue penetration of up to 5 cm in combination with high contrast and resolution, has a great potential to be clinically used for noninvasive, nonionizing visualization of a superficial organ such as the thyroid. In this study, we aim to show the use of biomarker-based photoacoustic imaging in the detection of follicular thyroid carcinoma in mice.

Several studies (6, 7) have suggested matrix metalloproteases as biomarkers that can differentiate between benign

Authors' Affiliations: [1]Canary Center at Stanford for Cancer Early Detection; [2]Molecular Imaging Program at Stanford, Department of Radiology and Bio-X Program, Stanford University, Palo Alto, California; [3]Department of Nuclear Medicine and Molecular Imaging, Ajou University School of Medicine, Suwon, Korea; and [4]Dom zdravlja Novi Beograd, Belgrade, Serbia

Corresponding Author: Sanjiv Sam Gambhir, Molecular Imaging Program at Stanford, James H. Clark Center, 318 Campus Drive, Stanford, CA 94305. Phone: 650-725-2309; Fax: 650-724-4948; E-mail: sgambhir@stanford.edu

American Association for Cancer Research

Translational Relevance

Current clinical thyroid cancer diagnosis relies on ultrasound and fine-needle aspiration cytology, both of which are unable to detect vascular and capsular invasion that is most often the only clear distinction between follicular thyroid carcinoma and adenoma. At present, the only method that can accurately diagnose follicular thyroid carcinoma is a biopsy after total or partial removal of the thyroid lobes. Only 20% to 30% of all biopsies diagnose malignancy, proving 70% to 80% of the surgical procedures as unnecessary. Having a non-invasive imaging method that could differentiate between benign and malignant follicular nodules would bring considerable benefit to patient management and reduce the healthcare costs by eliminating unnecessary surgeries. Photoacoustic imaging with good depth penetration in combination with high contrast and resolution has a great potential to be clinically used for noninvasive, nonionizing visualization of a superficial organ such as the thyroid.

Figure 1. Scheme illustrating the probe design and mechanism of action. Nonactivated probe produces a photoacoustic signal at 2 wavelengths (λ_{A1}, λ_{A2}) corresponding to the absorption maxima of the 2 chromophores A1 (BHQ3) and A2 (Alexa750). After cleavage, the CPP portion of the probe, carrying one of the chromophores, accumulates in cells and results in a photoacoustic signal at only 1 of the 2 wavelengths λ_{A1}. In the peptide, CXeeeeXPLGLAGrrrrrXK, small letters denote D-amino acids, X is a 6-aminohexanoyl acid.

and malignant thyroid lesions. Using immunohistochemistry and *in situ* hybridization, Cho Mar and colleagues detected significantly higher levels of MMP-2, MMP-7, and MMP-9 in patient tissues with minimally invasive follicular carcinoma than in adenoma and adenomatous goiter tissues. Buergy and colleagues (7) reported increased levels of MMP-1 and MMP-9 in patient tissues with follicular thyroid carcinoma as determined by ELISA. Matrix metalloproteinases, especially MMP-2 and MMP-9, are also known to be closely associated with tumor progression and aggressiveness (8–10).

We have recently reported the synthesis and cell culture testing of an MMP-activatable photoacoustic probe that showed more than 13-fold higher photoacoustic signal in cells exposed to the MMP-activated probe over the ones exposed to the nonactivated, uncleaved probe (11). Activatable probes, agents that provide signal only after the activation by their target, have attracted great attention in the field of molecular imaging as they offer higher sensitivity and specificity of detection than the conventional, "always on" probes (12). Our activatable photoacoustic probe is based on dual-wavelength imaging (Fig. 1). Before reaching its target, the probe shows photoacoustic signal of the ground state complex formed between the 2 absorbers (11). Although nonactivated probe shows signal at both wavelengths corresponding to the absorption maxima of the absorbers, the signals are similar in intensity and the subtraction of the photoacoustic signals obtained at the 2 excitation wavelengths makes the non-activated probe effectively photoacoustically silent. In the presence of a target, in this case, a matrix metalloproteinase enzyme, the probe is cleaved and the observed photoacoustic signal is of the separated absorbers. The absorber that is attached to the cell-penetrating peptide
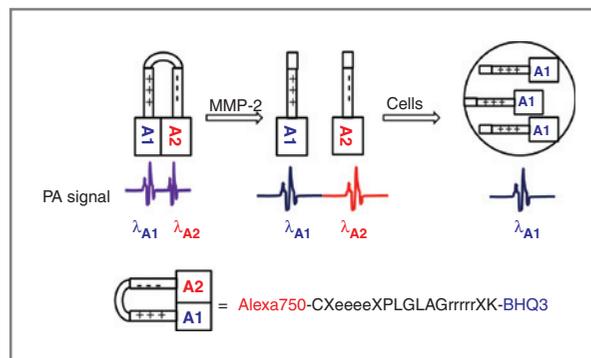
accumulates in nearby cells while the other absorber diffuses away, which, after the subtraction of the PA signal at the 2 excitation wavelengths, results in an increase in the photoacoustic signal.

The absorbers used in this study were a quencher, BHQ3, attached to the polyarginine, a cell-penetrating peptide part (CPP) of the molecule and a fluorescent molecule, Alexa750, connected to the polyglutamic acid chain that does not possess cell penetrating ability. The linker between CPP and polyglutamic acid chain was the peptide sequence, PLGLAG, shown to be preferentially cleaved by MMP-2 and MMP-9 (13).

Materials and Methods

Synthesis of the activatable B-APP-A and noncleavable, control probe

Black hole quencher BHQ3 NHS ester was purchased from Biosearch Technology, Alexa750 maleimide from Invitrogen, and the peptide prepared by Protein and Nucleic acid Facility at Stanford University (Stanford, CA). To the solution of approximately 1 mg peptide (active cleavable peptide, AcCXeeeeXPLGLAGrrrrrXK-CONH2 or noncleavable control consisting of D-amino acids AcCXeeeeXpl-GlagrrrrrXK-CONH2) in 500 µL PBS was added a solution of 500 µg BHQ3-NHS ester dissolved in 500 µL DMF and solution of 500 µg Alexa750 maleimide in 500 µL DMF. After leaving it for 2 hours at room temperature, the reaction mixture was directly injected onto high-performance liquid chromatography (HPLC) column. Analysis and purification of the probe were conducted using the Dionex Summit HPLC system (Dionex Corporation). Reverse-phase HPLC column Higins Analytical (Higins Analytical; C18, 4.6 mm × 250 mm) was used for the analysis of the reaction mixture. The mobile phase was 0.1% trifluoroacetic acid (TFA) in water (solvent A) and 0.1% TFA in 90% acetonitrile (CH_3CN) in water (solvent B). The products were detected by following absorbance at 675 and 750 nm. Matrix-

assisted laser desorption/ionization mass spectrometry (MALDI/MS) was conducted by the Canary Center proteomics facility on AB Sciex 5800 TOF/TOF System. The probes had a retention time of 18.6 minutes and a molecular mass of 4,015.11 (Supplementary Fig. S1 for information). The concentrations of the probes for all experiments bellow were calculated using Alexa750 extinction coefficient and absorbance at 750 nm (Supplementary Fig. S2).

In vitro MMP activity study

Active MMP-2 and MMP-9 were from EMD Chemicals. To the probe solution (0.2 nmol/100 μL PBS), various amounts of MMP-2 and MMP-9 were added and the mixture kept at 37°C for 1 hour. The change in fluorescence was recorded using Fluoromax 4 (Horiba Scientific). The excitation wavelength was 700 nm and fluorescence was detected in the 720- to 800-nm window.

Photoacoustic imaging of the probe cleavage in vitro

The active and the control probe (∼0.6 nmol) were each dissolved in 200 μL PBS and the solution split into 2 vials. After adding 0.2 μg of active MMP-9 to one of the vials, the solutions were kept at 37°C for 2 hours. Subsequent fluorescence measurements ($\lambda_{ex} = 720$ nm) revealed increase in fluorescence only in the solution containing active probe and MMP-9 enzyme. Increase in fluorescence was not observed for the solution of the control probe with MMP-9 indicating the probe was not being cleaved by the enzyme. The solutions were injected into capillary polyethylene tubes and embedded in 1% agar. Photoacoustic imaging was conducted using 680 and 750 nm wavelengths using a Visual Sonics Vevo LAZR system. To observe the probe cleavage photoacoustic images recorded at 750 nm were subtracted from the images obtained at 680 nm ($PA_{680nm} - PA_{750nm}$).

Determination of MMP-2 and MMP-9 levels in FTC133 tumors

MMP-2 and MMP-9 assay kits were purchased from GE Healthcare. For determination of the enzyme levels in tumors, tumors were excised from mice when they reached approximately 2 to 3 mm diameter in size, sonicated in Tris-HCl (pH 7.4) buffer, and the suspension centrifuged at 4°C and 2,000 × g for 10 minutes. The absorbance of the supernatant at 280 nm was used to standardize samples by the amount of total protein.

Optical imaging of the probe activation in vivo

All animal studies were conducted in accordance with the Guidelines for the Care and Use of Research Animals established by the Stanford University. Optical imaging of tumor-bearing mice ($n = 3$ for cleavable B-APP-A, $n = 3$ for the control probe) was conducted using an IVIS200 system (Caliper Life Sciences). The mice were intravenously injected with 1.3 nmol or intratumorally with 0.15 nmol of the probe and imaged using ICG filter set. The exposure time for images was 1 second. Quantitative analysis was conducted using the Living Image 4.0 software.

Photoacoustic imaging of the B-APP-A activation in vivo after intratumoral probe injection

Mice bearing FTC133 tumors ($n = 3$ for B-APP-A, $n = 3$ for the control probe) were photoacoustically imaged using a dedicated small-animal high-resolution imaging system (VevoLAZR; VisualSonics). A 256-element linear array transducer with center frequency of 21 MHz and spatial resolution of 75-μm resolution was placed to position the 10-mm focal depth in the center of the tumor. The photoacoustic gain was kept at 43 dB and dynamic range at 20 dB for all studies. The laser energy was recorded before and after each scan, and information used to normalize photoacoustic signal at different wavelengths. Ultrasound and photoacoustic images were obtained sequentially. Tumors were imaged using 680 and 750 nm laser light, before and 90 minutes after the intratumoral injection of 0.6 nmol probe.

Images were exported as 3-dimensional volume tiff files that were stacked together using ImageJ. Normalization of the images by the laser energy as well as subtraction of the images recorded at 680 and 750 nm were also done in ImageJ. Quantification was done using AMIDE software (14) using volumetric ellipsoid ROIs drawn based on the ultrasound images. Photoacoustic signal of the probe cleavage was obtained by subtracting images recorded at 680 and 750 nm at 90 minutes postinjection and normalizing the resulting subtraction image by the preinjection subtraction image $[(PA_{680nm} - PA_{750nm})_{postinjection}/(PA_{680nm} - PA_{750nm})_{preinjection}]$.

Photoacoustic imaging of the B-APP-A activation in vivo after tail vein probe injection

Mice bearing FTC133 tumors ($n = 5$ for B-APP-A, $n = 4$ for control probe) were photoacoustically imaged using a commercial Endra photoacoustic computed tomographic (PACT) system. The system uses a tunable nanosecond pulsed laser (7 ns pulses, 20-Hz pulse repetition frequency, about 7 mJ/pulse on the animal surface, wavelength range, 680–950 nm) and 128 unfocused ultrasound transducers (with 5 MHz center frequency and 3 mm diameter) arranged in a hemispherical bowl filled with water. We optimized imaging protocol to suit our probe experiments using 100 views and 100 pulses/view for each wavelength (680 and 750 nm). This protocol takes 18.9 minutes to acquire the data for both wavelengths. For each animal, we first obtained precontrast data at 680 and 750 nm. After tail vein administration of the probe (4.8 nmol), we continuously acquired data at the 2 wavelengths for 140 minutes. Volume-rendered 3D photoacoustic images are reconstructed off-line using data acquired from all 128 transducers from all views using a filtered back-projection algorithm. The algorithm corrects for pulse-to-pulse variations in the laser intensity and small changes in the temperature that affect acoustic velocity in the water. The reconstructed 3D raw data are then analyzed using AMIDE software (14). Photoacoustic signal of the probe cleavage was obtained by subtracting images recorded at 680 and 750 nm at a specific time

postinjection and normalizing the resulting subtraction image by the preinjection subtraction image [$(PA_{680nm} - PA_{750nm})_{postinjection}/(PA_{680\ nm} - PA_{750\ nm})_{preinjection}$].

Results

The activation of the B-APP-A probe by MMP-2 and MMP-9 *in vitro*

In our previous work (11), we observed static quenching between the 2 chromophores of the activatable probe, BHQ3-APP-Alexa750 (B-APP-A). Although there is no spectral overlap between the quencher ($\lambda_{max} = 675$ nm) and the fluorophore ($\lambda_{max} = 750$ nm), due to static quenching, the probe in its intact state shows very low fluorescence. The absorption and photoacoustic signal of the probe are also indicative of the ground state complex formed by the dimerization of the chromophores. The cleavage of the probe can be followed optically as we observe the increase in fluorescence due to the separation of Alexa 750 from the quencher. The probe was more efficiently cleaved by MMP-9 than by MMP-2 (Fig. 2A). We observed close to a 9-fold increase in fluorescence intensity after incubation of the probe with 0.1 µg of MMP-9 for 1 hour at 37°C. The same amount of probe required 20 times higher quantity of MMP-2 to achieve the same level of increase in fluorescence intensity (Fig. 2B). Besides MMP-2 and 9, PLGLAG sequence is known to be cleaved by other members of the MMP family (13). MMP-7 and MMP-13 that are also associated with thyroid cancer (7, 15) have shown good cleavage profiles,

although they were both less efficient than MMP-9 (Supplementary Fig. S3).

To show that the activation of the probe *in vitro* can be followed photoacoustically, we created an agar phantom with embedded tubes carrying solutions of the active and the control probes before and after the cleavage with MMP-9 (Fig. 2D and E). Increase in subtraction photoacoustic signal ($PA_{680nm} - PA_{750nm}$) was observed only for the active B-APP-A probe exposed to MMP-9. This result shows that cleavage only, without removal of Alexa 750 leads to the increase in subtraction signal (Fig. 2E).

MMP-2 and MMP-9 levels in FTC133 tumor homogenates

We chose to study the activation of the probe in follicular thyroid carcinoma using a FTC133 tumor model. Levels of MMP-2 and MMP-9 in tumor homogenates were determined using an immunocapture assay (16).

Active forms of both MMP-2 and MMP-9 were observed in tumor homogenates (Fig. 3) with MMP-9 detected in greater amount. Determination of the total enzyme level that includes both the proactive and the active forms suggested the predominance of the active form of MMP-9 in follicular tumors (Supplementary Fig. S4). Although cleaved by both enzymes, considering higher level of the active form of MMP-9 in tumor homogenates and the better cleavage efficiency (Fig. 2), we expect the probe to be primarily cleaved by the MMP-9 in FTC133 tumors.

Figure 2. The activation of the B-APP-A probe by MMP-2 and MMP-9 *in vitro*. The probe was more efficiently cleaved by MMP-9 (0.1 µg) than by MMP-2 (0.1 µg) enzyme (A). Complete cleavage of the probe as judged by the largest increase in fluorescence intensity was achieved using 2 µg MMP-2 (B) and 0.1 µg MMP-9 (C). The cleavage of the active and the control probes with MMP-9 was tested by fluorescence (D) and imaged photoacoustically (E). Polyethylene tubes containing approximately 0.6 nmol of the active and the control probes with and without MMP-9 were embedded in agar phantom (brightfield image shown on the left in E) and imaged using light of 680 and 750 nm wavelength. The subtraction image (680–750 nm) showed PA signal only in the capillary tubes carrying active probe, B-APP-A and MMP-9.
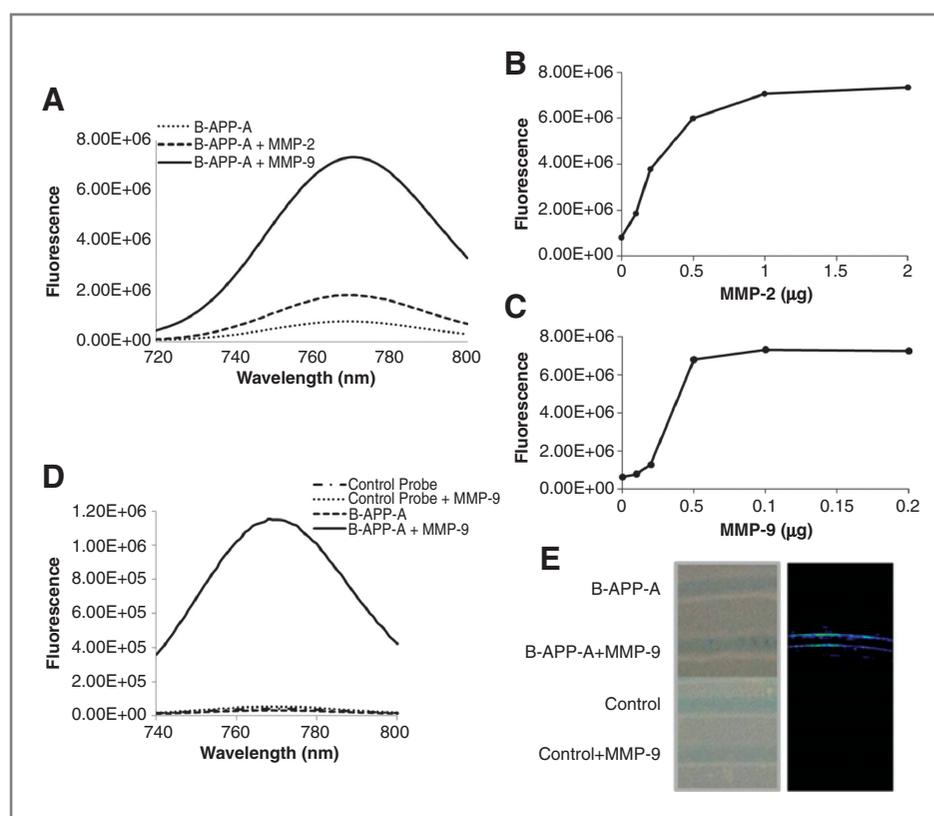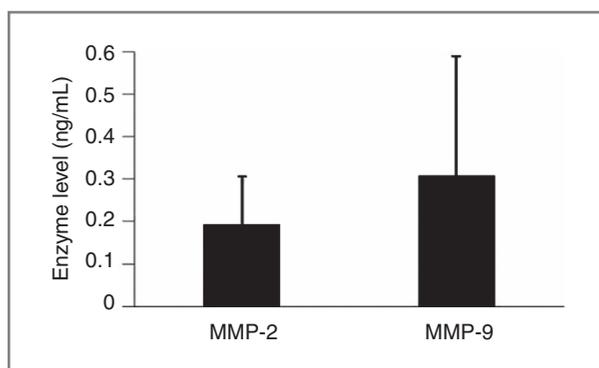
Figure 3. MMP-2 and MMP-9 levels in FTC133 tumor homogenates. Tumor homogenates had higher level of MMP-9 present. MMP-9 existed in predominately active form (Supporting Information). The error bars represent SD ($n = 3$).

Optical imaging of the probe activation *in vivo*

Because the probe cleavage produces both photoacoustic and fluorescent signal (Fig. 2), we were able to follow activation of the probe using optical imaging (Fig. 4). It needs to be stressed that the probe was not designed for fluorescent imaging as the chromophore that accumulates in cells is a quencher that is not detectable via optical imaging. However, the cleavage of the probe can still be followed optically by detecting the fluorescence of the fluorophore, Alexa 750 as it detaches from the quencher and clears away. Mice bearing follicular thyroid tumors were injected with the active probe B-APP-A and the control, a noncleavable probe having the same peptide sequence but composed of D-amino acids. Fluorescence signal at the tumor site of mice injected with the control probe was significantly lower than the fluorescence signal in mice injected with the active probe (Fig. 4A and B). High fluorescent signal was observed in the kidneys signifying probable clearance route (Supplementary Fig. S5). Similar results were observed in the study that investigated proteolytic activation of a related cleavable peptide by optical imaging (17). The clearance through and possible accumulation in the kidneys could lead to systemic toxicity hypothesized to result from the nonspecific cleavage of the probe followed by mast cell degranulation (13). Systemic toxicity could be minimized by reducing the nonspecific cleavage through containment of the probe proteolysis within tumor
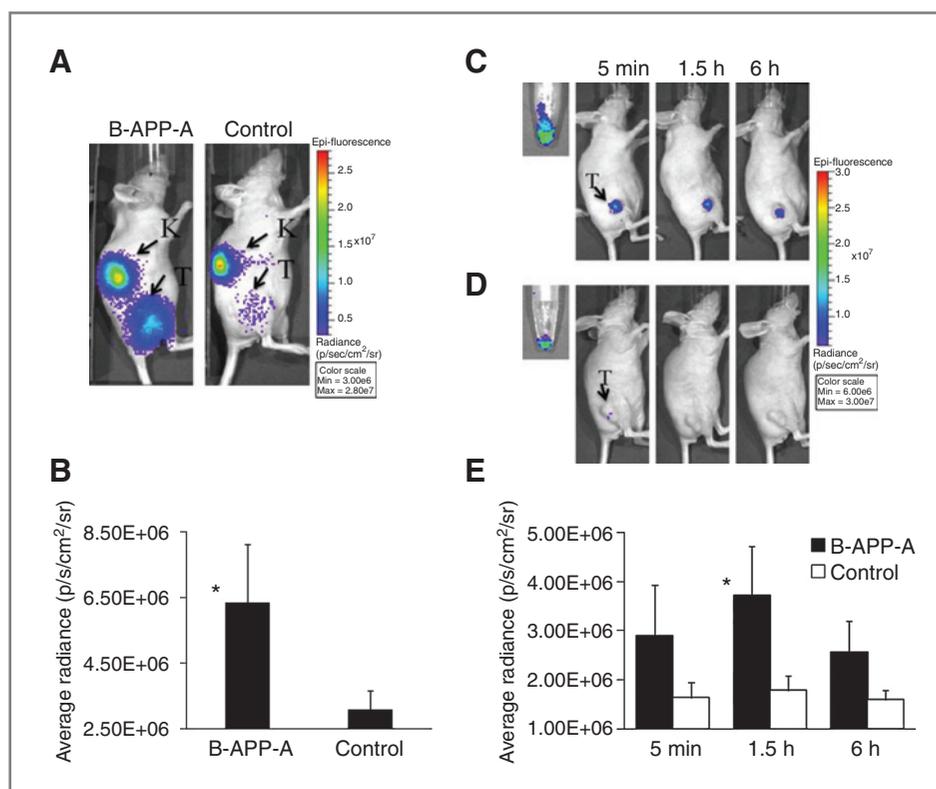

Figure 4. Optical imaging of the probe activation in FTC133 tumors. Mice bearing FTC133 tumors in the hind legs were intravenously injected with 1.3 nmol of the B-APP-A or the control probe and optically imaged using ICG filter set (710–760 nm excitation and 810–875 nm emission) with 1-second exposure time. A, one and a half hours postinjection there was a considerably higher fluorescent signal in the tumors of mice injected with the cleavable B-APP-A probe than in the mice injected with the control probe. B, quantitative analysis revealed 2-fold higher fluorescent signal in the tumors of mice injected with the B-APP-A probe than of the mice injected with the control probe. The error bars represent SD. *, $P < 0.05$, $n = 3$. Intratumoral injection of 0.15 nmol of the B-APP-A (C) and the control probe (D) was optically imaged using ICG filter set (710–760 nm excitation and 810–875 nm emission) with 1s exposure time. E, one and a half hours postinjection, there was a significantly higher fluorescent signal in the tumors of mice injected with the cleavable B-APP-A probe than in tumor of mice injected with the control probe. Error bars represent SD ($n = 3$). *, $P < 0.05$. The small images in C and D are fluorescent images of the B-APP-A control probe before intratumoral injection and show the same level of fluorescence intensity for both probes.

by means of intratumoral injections or by improving pharmacokinetic behavior through attachment of macromolecules, such as polyethylene glycol, to the probe to minimize renal clearance (18).

We tested the intratumoral activation of the probe by injecting 0.15 nmol of the probe directly into FTC133 tumors and following the fluorescence increase over time (Fig. 4C and D). Fluorescence signal obtained from the tumors injected with the cleavable probe was higher than the signal detected in the tumors injected with the control probe at all time points becoming significantly different at 1.5 hours postinjection.

Photoacoustic imaging of the probe activation in living mice

Tumors were photoacoustically imaged using 680 and 750 nm light, before and 90 minutes after injecting 0.6 nmol probe directly into the tumor. The preinjection images served as normalization factors for our postinjection images. Signal acquired at 750 nm was subtracted from the signal recorded at 680 nm to obtain photoacoustic signal corresponding to the cleavage of the probe. Tumors injected with the active probe showed significantly higher normalized subtraction PA signal than the tumors injected with the control probe (Fig. 5A and B). It needs to be pointed out here that the injection of either of the probes leads to increase in photoacoustic signal at individual wavelength (Supplementary Fig. S6). The difference between the 2 probes caused by the cleavage became apparent only upon subtraction of the images acquired at 680 and 750 nm.

Thyroid tumors were also photoacoustically imaged continuously for 140 minutes after the tail vein injection of 4.8 nmol of the probes (Fig. 6). At early time points, we did not observe any difference between active and control probe. Over time, the signal for active probe increased steadily,

becoming significantly different than the signal for the control probe at 100 minutes postinjection (Fig. 6B).

Discussion

The targets that we investigated were extensively studied members of the matrix metalloproteinase family, MMP-2 and MMP-9, which have been suggested as markers able to distinguish between follicular thyroid carcinoma and adenoma (6, 7). Using quantitative immunocapture assay, we have determined MMP-9 to be the dominant form in FTC133 tumors.

In a recent study, Razansky and colleagues (19) used multispectral optoacoustic tomography to image atherosclerotic plaques *ex vivo* using commercially available MMP-activated probe MMPSense 680 intended for optical imaging. In the current study, we used photoacoustic probe based on dual-wavelength imaging activated by the MMP cleavage of the peptide linker. On the basis of the efficiency of the proteolysis and the high quantities of the active form present in FTC133 tumors, we expect the probe to be preferentially activated by MMP-9 in living subjects.

Two recent studies (20, 21) have reported possible nonspecific cleavage for probes of similar design that would lead to diminished target specificity of our probe. One study suggested the breakdown of the BHQ3 in blood plasma, rather than the MMP cleavage of the probe, to be a process that leads to the fluorescence emission (21). Optical imaging of tumor-bearing mice injected with the active and the control probe gave insight into the extent and rate of BHQ3 breakdown in our probe. Similarly to the MMP cleavage, the breakdown of the BHQ3 would result in the increase in fluorescence, and if it were a preferential activation process, the same level of fluorescence should be observed for both the active and the control probe. Because we observed a 2-fold higher fluorescence signal in mice injected with the
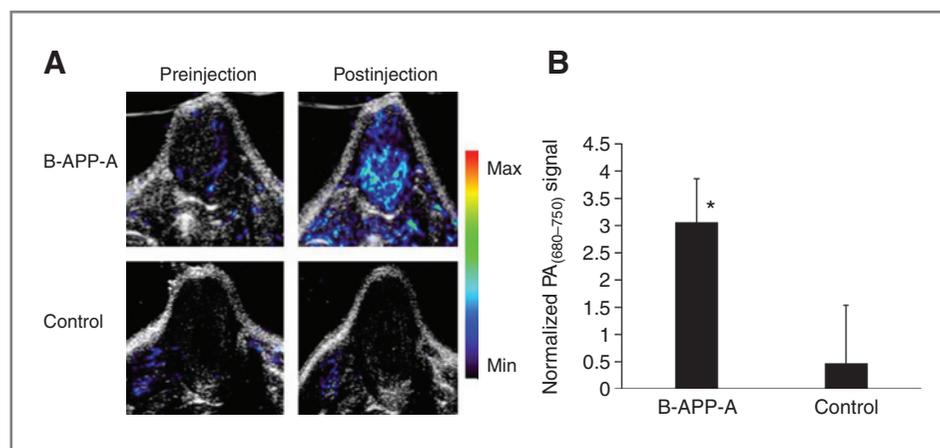

Figure 5. Photoacoustic imaging of the probe activation in tumor after intratumoral injection of the probe. Mice bearing FTC133 tumors in the hind legs were photoacoustically imaged using 680 and 750 nm light before and after the intratumoral injection of 0.6 nmol B-APP-A or the control probe (A). Gray outline represents the ultrasound image of the tumor, whereas the rainbow scale corresponds to the detected photoacoustic signal. At 90 minutes postinjection, the subtraction of the images at the 2 wavelengths led to a clear increase in photoacoustic signal for the active probe. The increase in signal was not observed after the injection of the control probe. Quantification of the photoacoustic signal showed significantly higher signal after injection of the cleavable probe than after injection of the control probe. Subtraction photoacoustic signal was normalized by the preinjection subtraction photoacoustic signal $[(PA_{680\ nm} - PA_{750\ nm})_{90\ min\ postinjection}/(PA_{680\ nm} - PA_{750\ nm})_{preinjection}]$. The error bars represent SD ($n = 3$; *, $P < 0.05$).
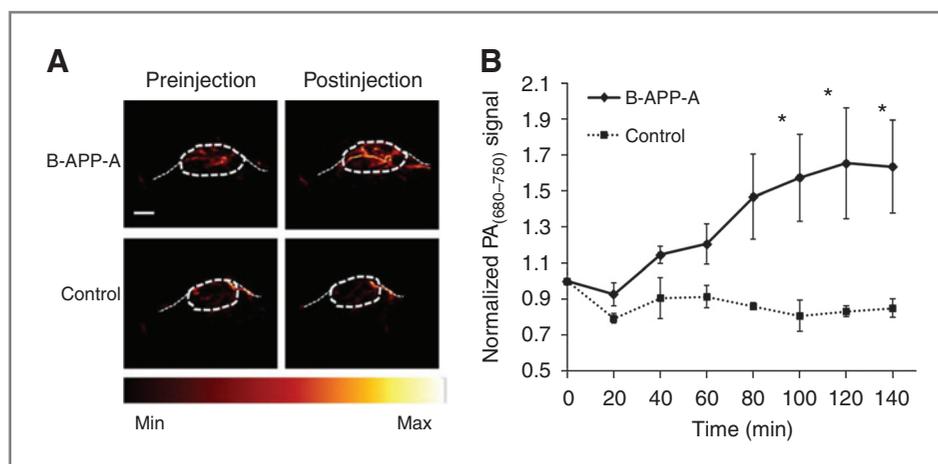
Figure 6. Photoacoustic imaging of the probe activation in tumor after tail vein injection of the probe. Mice bearing FTC133 tumors in the hind legs were photoacoustically imaged using 680 and 750 nm light before and after the injection of 4.8 nmol of the B-APP-A and the control probe (A). The subtraction photoacoustic signal at 140 minutes postinjection was approximately 1.7-fold higher than the preinjection signal for the active probe. The subtraction signal for the control probe did not change over time. At early time points, the difference in subtraction signal was not significantly different for the two probes. Over time the signal for activatable probe steadily increased, becoming significantly different at 100 minutes (B). Subtraction photoacoustic signal was normalized by the preinjection subtraction photoacoustic signal $[(PA_{680\ nm} - PA_{750\ nm})_{postinjection}/(PA_{680\ nm} - PA_{750\ nm})_{preinjection}]$. The error bars represent SE ($n = 5$ for B-APP-A, $n = 4$ for control probe; *, $P < 0.05$). Scale bar is 0.25 cm.

active probe, we reason that at this time point, the breakdown of BHQ3 was not contributing significantly to the increase in fluorescence signal. The other study by van Duijnhoven and colleagues pointed to a possibility of a nonspecific tumor accumulation of the probe caused by the tumor-independent activation most likely occurring in the vasculature (20). Although this study reported results only at one time point, 24 hours postinjection, when the nonspecific cleavage contribution may be more significant than at earlier time points at which we image, to minimize any possible nonspecific cleavage, we investigated direct intratumoral injections. The direct local delivery of the imaging probe should not present a problem as thyroid nodules are easily accessed using well-established clinical method, ultrasound guided fine-needle aspiration. Intranodular injections would localize activation of the probe and would thus provide the information on the MMPs activity only in the nodule. In addition, the study by Lo and colleagues suggested that intratumoral injection would minimize any BHQ3 breakdown as they reported very little nonspecific cleavage 24 hours after intratumoral injection of the BHQ3-labeled peptide (22).

Optical imaging of mice intratumorally injected with the active and the control probe suggested 90 minutes postinjection to be the optimal time for imaging the difference in cleavage between the 2 probes. The signal coming from the tumors injected with the cleavable probe was higher at all time points than the signal from the tumors injected with the noncleavable probe. While the signal for the B-APP-A probe increased over 90 minutes and then slowly decreased at 6 hours postinjection, the control probe had a stable fluorescent signal decreasing at a slower rate. The increase in fluorescence observed at 90 minutes for B-APP-A probe can be attributed to the cleavage of the probe and release of Alexa 750 from the

ground complex. Being smaller than the intact probe, the polyanionic part carrying Alexa 750 clears more efficiently from the tumor site causing a drop in the fluorescence intensity. The fluorescent signal of the control probe shows slower decay as a result of the intact probe's delayed clearance. The fluorescent signal in the bladder of B-APP-A injected mice was considerably higher than the signal in control probe injected mice suggesting differential clearance between the 2 probes (Supplementary Fig. S7).

Although the similarity of the difference in fluorescence increase between the active and the control agent after intravenous and intratumoral injection (2.06- vs. 2.09-fold, Fig. 4C and D) suggested there was no tumor nonspecific activation at the time point of imaging, we investigated photoacoustic imaging of tumors after intranodular injection because that strategy is clinically feasible and can provide reduction in potential systemic toxicity. Photoacoustic imaging after intratumoral injection showed clear distinction between tumors injected with the active and the control probe.

Continuous photoacoustic imaging after tail vein injection clearly differentiated between the 2 probes. At early time points after the injection, the active and the control agent showed similar photoacoustic signal as there was no appreciable accumulation of the quencher in tumors. Over time, with more active probe being cleaved by the MMPs, higher levels of the quencher accumulated at the cleavage site leading to an increase in the photoacoustic signal. Because the control probe cannot be cleaved, it cleared away from the tumor site without significant accumulation of the quencher resulting in no increase in photoacoustic signal over time. Significant difference in signal between the active and the control probe was observed 100 minutes postinjection, which represents the time suitable to image

MMP activity. Although for clinical translation the optimal imaging time would have to be redetermined, the imaging time point of 100 minutes postinjection in mice indicates that in humans the most favorable imaging time would be within clinically relevant time of few hours postinjection of the probe. The difference between the active and the control probe was more pronounced after the intratumoral injection than after the intravenous one, most likely because of the differential pharmacokinetic behavior. Because it is circulating in the blood, only a portion of the intravenously injected active probe gets cleaved in the tumors. On the other hand, intratumoral injections confine the probe to the tumor and slow down its clearance allowing more time for the cleavage and accumulation. The images in Figs. 5 and 6 effectively illustrate the superior resolution achieved with photoacoustic imaging. Although optical imaging provides information about MMP activation as well (Fig. 4), the details about the exact location of the signal are lacking.

There are several issues that need to be addressed in the future studies. Both fluorescent and photoacoustic signal in tumors intratumorally injected with the imaging probes varied greatly between mice. Nonuniform intratumoral injection was likely a major reason for the observed variation. A more efficient intratumoral delivery method will likely be needed to minimize this variation. In addition, although we investigated the cleavage of the probe in non-thyroid tumors with high and low MMP levels (Supplementary Fig. S8), because of the lack of good animal models for thyroid adenomas, we did not evaluate the probe in benign tumors. To show the ability of the probe to differentiate between carcinomas and adenomas, in future studies, we plan to expose the probe to normal and cancer tissue extracts as sources with differential levels of MMPs. The planned study will also be used to correlate the level of MMPs to the photoacoustic signal, a link that needs to be determined for a complete quantitative evaluation of the use of the biomarker-based molecular imaging strategy.

In conclusion, we report here the photoacoustic molecular imaging of the follicular thyroid carcinoma using an activatable photoacoustic probe. A large variety of photoacoustic agents, mainly nanoparticles, have been developed and used in various imaging applications (23–26). To the best of our knowledge, this the first report of the use of a small-molecule–based activatable photoacoustic probes in living subjects. The agent was efficiently cleaved by the MMPs and the activation as well as the subsequent accumulation successfully photoacoustically imaged. Offering a combination of the high spatial resolution and signal specificity, targeted photoacoustic molecular imaging holds great promise as a noninvasive method for diagnosing follicular thyroid carcinomas.

Disclosure of Potential Conflicts of Interest

S.S. Gambhir is employed (other than primary affiliation; e.g., consulting) in Endra as a board member and has ownership interest (including patents) and is a consultant/advisory board member of Visualsonics. No potential conflicts of interest were disclosed.

Authors' Contributions

Conception and design: J. Levi, J.-K. Yoon, D. Starcevic, S.S. Gambhir
Development of methodology: J. Levi, A. Tisma, S.S. Gambhir
Acquisition of data (provided animals, acquired and managed patients, provided facilities, etc.): J. Levi, S.-R. Kothapalli, S. Bohndiek, J.-K. Yoon, C. Nielsen, G. Gowrishankar, C. Chan
Analysis and interpretation of data (e.g., statistical analysis, biostatistics, computational analysis): J. Levi, S.-R. Kothapalli, S. Bohndiek, S.S. Gambhir
Writing, review, and/or revision of the manuscript: J. Levi, S.-R. Kothapalli, S. Bohndiek, C. Nielsen, A. Tisma, C. Chan, D. Starcevic, S.S. Gambhir
Administrative, technical, or material support (i.e., reporting or organizing data, constructing databases): J. Levi, S.-R. Kothapalli, A. Dragulescu-Andrasi, S. Bodapati, X. Yan, S.S. Gambhir
Study supervision: J. Levi, S.-R. Kothapalli, S.S. Gambhir

References

1. SEER Cancer Statistics Review 1975–2009 [cited 2012 Oct 10]. Available from: http://seer.cancer.gov/csr/1975_2009_pops09/results_merged/sect_26_thyroid.pdf.
2. Goldstein RE, Netterville JL, Burkey B, Johnson JE. Implications of follicular neoplasms, atypia, and lesions suspicious for malignancy diagnosed by fine-needle aspiration of thyroid nodules. Ann Surg 2002;235:656–62; discussion 62-4.
3. Massoud TF, Gambhir SS. Integrating noninvasive molecular imaging into molecular medicine: an evolving paradigm. Trends Mol Med 2007;13:183–91.
4. Massoud TF, Gambhir SS. Molecular imaging in living subjects: seeing fundamental biological processes in a new light. Genes Dev 2003;17:545–80.
5. Li C, Wang LV. Photoacoustic tomography and sensing in biomedicine. Phys Med Biol 2009;54:R59–97.
6. Cho Mar K, Eimoto T, Tateyama H, Arai Y, Fujiyoshi Y, Hamaguchi M. Expression of matrix metalloproteinases in benign and malignant follicular thyroid lesions. Histopathology 2006;48:286–94.
7. Buergy D, Weber T, Maurer GD, Mudduluru G, Medved F, Leupold JH, et al. Urokinase receptor, MMP-1 and MMP-9 are markers to differentiate prognosis, adenoma and carcinoma in thyroid malignancies. Int J Cancer 2009;125:894–901.
8. Coussens LM, Fingleton B, Matrisian LM. Matrix metalloproteinase inhibitors and cancer: trials and tribulations. Science 2002;295:2387–92.
9. Omi Y, Shibata N, Okamoto T, Obara T, Kobayashi M. The role of CD147 in the invasiveness of follicular thyroid carcinoma cells. Thyroid 2012;22:383–94.
10. Kraiem Z, Korem S. Matrix metalloproteinases and the thyroid. Thyroid 2000;10:1061–9.
11. Levi J, Kothapalli SR, Ma TJ, Hartman K, Khuri-Yakub BT, Gambhir SS. Design, synthesis, and imaging of an activatable photoacoustic probe. J Am Chem Soc 2010;132:11264–9.
12. Kobayashi H, Choyke PL. Target-cancer-cell-specific activatable fluorescence imaging probes: rational design and *in vivo* applications. Acc Chem Res 2011;44:83–90.

13. Aguilera TA, Olson ES, Timmers MM, Jiang T, Tsien RY. Systemic *in vivo* distribution of activatable cell penetrating peptides is superior to that of cell penetrating peptides. Integr Biol (Camb) 2009;1: 371–81.

14. Loening AM, Gambhir SS. AMIDE: a free software tool for multimodality medical image analysis. Mol Imaging 2003;2:131–7.

15. Baldini E, Toller M, Graziano FM, Russo FP, Pepe M, Biordi L, et al. Expression of matrix metalloproteinases and their specific inhibitors in normal and different human thyroid tumor cell lines. Thyroid 2004; 14:881–8.

16. Smith L MA, Capper SJ. Determination of species cross-reactivity using MMP-2 Activity Assay and correlation with ELISA and gelatin zymography. Life Science News 1999;3:1–2.

17. Jiang T, Olson ES, Nguyen QT, Roy M, Jennings PA, Tsien RY. Tumor imaging by means of proteolytic activation of cell-penetrating peptides. Proc Natl Acad Sci U S A 2004;101:17867–72.

18. Olson ES, Aguilera TA, Jiang T, Ellies LG, Nguyen QT, Wong EH, et al. *In vivo* characterization of activatable cell penetrating peptides for targeting protease activity in cancer. Integr Biol (Camb) 2009;1: 382–93.

19. Razansky D, Harlaar NJ, Hillebrands JL, Taruttis A, Herzog E, Zeebregts CJ, et al. Multispectral optoacoustic tomography of matrix metalloproteinase activity in vulnerable human carotid plaques. Mol Imaging Biol 2012;14:277–85.

20. van Duijnhoven SM, Robillard MS, Nicolay K, Grull H. Tumor targeting of MMP-2/9 activatable cell-penetrating imaging probes is caused by tumor-independent activation. J Nucl Med 2011;52:279–86.

21. Linder KE, Metcalfe E, Nanjappan P, Arunachalam T, Ramos K, Skedzielewski TM, et al. Synthesis, *in vitro* evaluation, and *in vivo* metabolism of fluor/quencher compounds containing IRDye 800CW and Black Hole Quencher-3 (BHQ-3). Bioconjug Chem 2011;22:1287–97.

22. Lo PC, Chen J, Stefflova K, Warren MS, Navab R, Bandarchi B, et al. Photodynamic molecular beacon triggered by fibroblast activation protein on cancer-associated fibroblasts for diagnosis and treatment of epithelial cancers. J Med Chem 2009;52:358–68.

23. Jokerst JV, Thangaraj M, Kempen PJ, Sinclair R, Gambhir SS. Photoacoustic imaging of mesenchymal stem cells in living mice via silica-coated gold nanorods. ACS Nano 2012;6:5920–30.

24. Homan KA, Souza M, Truby R, Luke GP, Green C, Vreeland E, et al. Silver nanoplate contrast agents for *in vivo* molecular photoacoustic imaging. ACS Nano 2012;6:641–50.

25. Li W, Brown PK, Wang LV, Xia Y. Gold nanocages as contrast agents for photoacoustic imaging. Contrast Media Mol Imaging 2011;6: 370–7.

26. de la Zerda A, Bodapati S, Teed R, May SY, Tabakman SM, Liu Z, et al. Family of enhanced photoacoustic imaging agents for high-sensitivity and multiplexing studies in living mice. ACS Nano 2012;6:4694–701.

Clinical Cancer Research

Molecular Photoacoustic Imaging of Follicular Thyroid Carcinoma

Jelena Levi, Sri-Rajashekar Kothapalli, Sarah Bohndiek, et al.

Updated version	Access the most recent version of this article at: doi:10.1158/1078-0432.CCR-12-3061
Supplementary Material	Access the most recent supplemental material at: http://clincancerres.aacrjournals.org/content/suppl/2013/01/24/1078-0432.CCR-12-3061.DC1

Cited articles	This article cites 25 articles, 4 of which you can access for free at: http://clincancerres.aacrjournals.org/content/19/6/1494.full#ref-list-1
Citing articles	This article has been cited by 7 HighWire-hosted articles. Access the articles at: http://clincancerres.aacrjournals.org/content/19/6/1494.full#related-urls

E-mail alerts	Sign up to receive free email-alerts related to this article or journal.
Reprints and Subscriptions	To order reprints of this article or to subscribe to the journal, contact the AACR Publications Department at pubs@aacr.org.
Permissions	To request permission to re-use all or part of this article, use this link http://clincancerres.aacrjournals.org/content/19/6/1494. Click on "Request Permissions" which will take you to the Copyright Clearance Center's (CCC) Rightslink site.